MethodsX 14 (2025) 103156

Contents lists available at ScienceDirect

MethodsX

journal homepage: www.elsevier.com/locate/methodsx

Upgrade of a variable temperature scanning tunneling microscope for nanometer-scale spectromicroscopy

B. Cirera[a,*], A. Sáez-Coronado[a], D. Arribas[a], J. Méndez[a], A. Sagwal[b,c], R. de Campos Ferreira[b], M. Švec[b,d], P. Merino[a,*]

[a] Material Science Institute of Madrid (ICMM-CSIC). c/ Sor Juana Inés de la Cruz 3, 28049, Spain
[b] Institute of Physics, Czech Academy of Sciences; Cukrovarnická 10/112, Praha 6 CZ16200, Czech Republic
[c] Faculty of Mathematics and Physics, Charles University; Ke Karlovu 3, CZ12116 Praha 2, Czech Republic
[d] Institute of Organic Chemistry and Biochemistry, Czech Academy of Sciences; Flemingovo náměstí 542/2, Praha 6 CZ160 00, Czech Republic

ARTICLE INFO

Method name:
Adjustable portable lens for scanning probe optical spectroscopy

Keywords:
Scanning Probe Microscopy (SPM)
Tip-Enhanced Raman Spectroscopy (TERS)
3D metal printing
Ultrahigh Vacuum (UHV) lens holder

ABSTRACT

Tip-enhanced Raman spectroscopy (TERS), tip-enhanced photoluminescence (TEPL), and scanning tunneling microscope-induced luminescence (STML) combine the high spatial resolution of probe microscopies with the spectroscopic capabilities of optical techniques. Here, we describe the upgrade of an ultrahigh vacuum (UHV) variable-temperature scanning probe microscope (VT-SPM) to perform tip-enhanced spectromicroscopy experiments at cryogenic temperatures. The home-made design includes a portable focusing lens (NA=0.45) that allows the simultaneous collection and injection of light from the tip-sample junction while assuring easy tip and sample transfers. We demonstrate the capabilities of our upgrade to resolve electroluminescence (EL), Raman, and TERS spectra using plasmonically active probes (Ag and Au tips) on various surfaces. We are able to observe the vibrational levels of C_{60} deposited on Ag(111) with a lateral resolution of ~2 nanometers. Moreover, we use the tunability of the gap plasmon distribution to observe intense anti-Stokes signals of C_{60}, highlighting the spectral sensitivity of the system. This upgrade opens new possibilities for studying surface chemistry, catalysis, and molecular electronics at state-of-the-art spatial and spectral resolutions using accessible SPM systems.

- Portable lens holder
- In-situ adjustable position
- Nanometer-scale vibrational spectroscopy

Specifications table	
Subject area:	Physics and Astronomy
More specific subject area:	*Scanning probe optical spectroscopy*
Name of your method:	Adjustable portable lens for scanning probe optical spectroscopy
Resource availability:	*STEP Files for the Lens holder, Slider and Support*

Background

Tip-enhanced spectromicroscopies in ultrahigh vacuum permit the characterization of optoelectronic processes down to the single bond limit [1,2]. In recent years, we have witnessed rapid advances profiting from plasmonic nanocavities, which have allowed,

* Corresponding authors
E-mail addresses: borja.cirera@csic.es (B. Cirera), pablo.merino@csic.es (P. Merino).

https://doi.org/10.1016/j.mex.2025.103156
Received 31 October 2024; Accepted 4 January 2025
Available online 7 January 2025

among other, to visualize plasmons, excitons, and vibrations with atomic resolution [3,4]. Most instruments intended for this purpose have specifically designed lenses or parabolic mirrors placed very close to the tip-sample junction with high numerical apertures (NA). However, many commercially available scanning probe instruments in laboratories worldwide lack such lens systems, though they could significantly benefit from upgrades that enable luminescence experiments. Interestingly, majority of these systems can be relatively easily upgraded by simple designs and commercial lenses [5]. The advent of affordable, UHV-compatible materials for 3D printing technologies has put an extremely versatile tool within our reach for creating advanced upgrades in commercial systems such as lens holders and adapters.

In this work we report an upgrade of a variable-temperature scanning probe microscope (VT-SPM) originally designed by Omicron GmbH, enabling a close focusing of the SPM junction, particularly suited to perform optical experiments. We achieve it by adding a practicable mobile lens system to the STM head, which can be retracted from the SPM tip-sample junction with the wobble stick included in the original SPM chamber. Moreover, this system allows for a precise fine-tuning of the focus using a simple lever mechanism. We demonstrate that this setup can precisely focus and collect light onto and from the junction on different supports, by investigating the plasmonic electroluminescence of noble-metal single crystals, measuring the micro-Raman scattering of silicon bulk phonon, and the tip-enhanced Raman spectroscopy of C_{60} molecular islands on Ag(111). Moreover, we are able to acquire TERS spectra with characteristic acquisition times in the order of seconds with lateral resolutions of a few nanometers, even being able of observing the anti-Stokes branch thanks to the spectral enhancement in the plasmonic nanocavity.

Method details

The VT-SPM Scienta Omicron is one of the most popular SPM for room- and variable-temperature applications. It has been commercialized for >20 years, with >500 instruments delivered and installed around the world [6]. With the advent of tip-enhanced spectroscopy in UHV, these instruments have shown enormous potential for performing routine as well as advanced experiments on bulk [7], thin films [8–10], molecular assemblies [11], and small molecules [12] presenting strong optical response in the 40–300 K range. However, the original design lacks an optical collection/illumination system for the tunnel junction or any possibility of upgrading for this purpose. The main element in luminescence experiments is a focusing device (typically a lens or a parabolic mirror) placed at a close distance (typically 10–20 mm) from the tip-sample junction. Due to the compactness of the VT-STM head, some limitations for upgrading arise. The only possibility for guiding light beams to the scanner without modification of the SPM head is through one of the evaporation paths present in the lower part of the system, namely the path approaching from the open front side of the sample stage. However, the presence of a fixed lens system in the sample stage would render the transfer and exchange of the sample in vacuum physically impossible, drastically affecting the performance of the setup.

We overcome these limitations by designing a vacuum compatible lens holder placed on a slider that moves on top of a monorail (Fig. 1a), whose corresponding STEP files are given in the supplementary material to facilitate their printing to other research groups. The system consists of three separate parts: the platform with the rail, the slider, and the lens holder. The final design of the assembly is based on the geometry of the STM head as depicted in Fig. 1b. The dimensions have been determined by carefully assessing the distances on the existing apparatus. The slider moves on the rail along a dovetail profile, and is embedded with magnetic latches to fix it in the retracted or measurement positions via two small magnets integrated into the rail and the slider (Fig. 1c and d). This design permits the approach of the lens to the junction for luminescence experiments and its retraction, leaving enough space for tip and sample exchanges. The commercial plastic aspheric lens has an effective focal length of 12 mm at 587.6 nm and a diameter of 12 mm, resulting in a NA of 0.50. However, due to the proximity of the lower part of the lens to the tip holder (central piezo tube) at operating conditions, 2 mm of the lens had to be removed by mechanical sanding, resulting in a slightly reduced effective NA to approximately 0.45. Plastic aspheric lenses are very light and represent an affordable option to correct the spherical aberration, while the material can be easily machined to suit the geometry of each particular SPM setup. The optical axis of the lens is at an angle of 30° with respect to the sample plane, coinciding with the angle of the optical/evaporation access path present in the original chamber. With this configuration, the lens covers ~ 14 % of the solid angle.

On the air side, the path is sealed with a CF40 transparent borosilicate window, to which the external optical cage system is anchored. The designed vertical position of the focal point is 3 mm below the rear side of the sample baseplate (h in Fig. 1b). It is intended for use with the standard 1 mm thick flag-style sample holders, with single crystals of 2 mm height. Our design allows for the use of single crystals with different heights by either using a conducting metallic spacer or reducing the sample holder thickness below the sample to adjust the total height to the desired 3 mm. Moreover, the slider enables the precise adjustment of the vertical position of the lens in vacuum by turning a screw with the wobble stick (orange arrow in Fig. 1b), presenting a stepless range of 2° and the resulting total adjustable height range of ~0.5 mm. This simple lever mechanism is actuated by moving the inner nut upwards as the screw is rotated clockwise (tighten), resulting in the movement of the lens holder (purple arrow in Fig. 1b).

The rail and the lens assembly are mounted on the STM head at the position marked by the overlap of the rectangular corners of the rail mount with the golden-plated base of the scanner, as highlighted in Fig. 1c with the white arrows. With this alignment, there is an unobstructed view of the tip-sample junction through the optical access, which allows the supervised initial coarse approach of the tip (Figure S1a). Afterwards, the slider is operated easily with the original wobble-stick into the measurement position (red arrow in Fig. 1c), where the fine approach and the focusing of the tip-sample junction is carried out through the focusing lens. Once the main components of the system are in position, the optical measurements can be carried out in tunneling conditions.

The exterior optical cage system is located close to the UHV window mounted on a X-Y adjustable plate, while the Z position remains static after anchoring (see Figure S1b for the integrated system), with the components of the optical setup depicted in Fig. 1e. We decided to install a compact cage system (Thorlabs), which permits an easy swapping of the static components such as

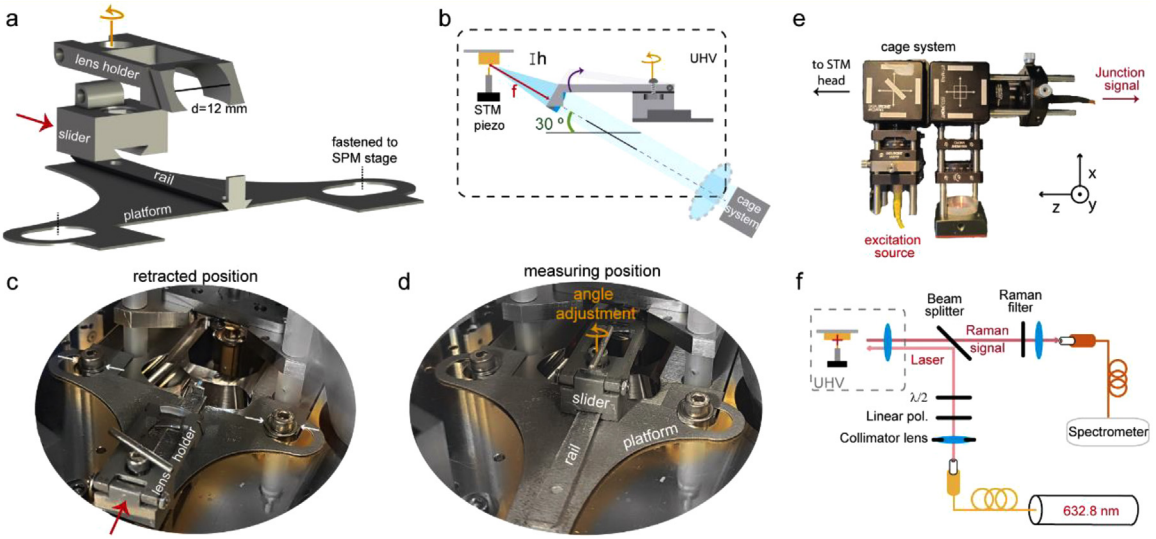

Fig. 1. a) View of the STEP file of our custom-designed mobile lens support, highlighting its three different structures: the anchoring point to the SPM platform, the angle-tuning mechanism (orange arrow) and the point where the wobble-stick pushes the slider to the measuring position (red arrow). b) Sketch of the lens support on the STM platform with respect to the tip-sample junction and the intended beam path. c) Picture of the SPM head with the lens holder in a retracted position away from the scanner to allow the sample transfer, with the point where it is actuated with the wobble-stick denoted by a red arrow. d) Picture of the lens holder and slider in the measurement position at the end of the rail, with the screw for fine angle-tuning highlighted in orange. The system is retracted to the position depicted in c by actuating on the upper part of the screw with the wobble-stick in the direction away from the scanner. e) Picture of the optical cage fiber focusing and camera system placed outside of the UHV environment. f) Scheme of the entire optical setup for excitation and detection of Raman scattering signal in the junction, noting that the Raman output path is identical for the STML measurements.

filters and mirrors, to change between different modes following our previous experience on a low temperature SPM system [13]. The signal output of the optical cage consists of an optical fiber adapter mounted on a X-Y stage to adjust the collection of the light emitted from the junction. This is connected by cage rods to the first cube cage, where we insert either a right-angle mirror cube during the camera focusing procedure or Raman filters during TERS measurements, while for electroluminescence experiments this cube is removed. The cube cage closer to the chamber can hold the beam splitter required for experiments with an excitation light source. The excitation signal is delivered by a single-mode optical fiber and then collimated with a lens mounted on a X-Y stage for fine alignment. The scheme of the optical setup optimized for TERS is shown in Fig. 1f (see Supporting Information Figure S2 for the configurations corresponding to photoluminescence and electroluminescence).

Method validation

Under measurement conditions, the tip geometry can be precisely observed through the lens, allowing the rough calculation of the mesoscopic radius of curvature for the different tips (example in Fig. 2a). All experiments presented here were performed in ultra-high vacuum conditions (base pressure $<5 \times 10^{-10}$ mbar). The scattered photons are collected by the inner lens and detected outside of the UHV chamber with a grating spectrometer (Andor Kymera 328i Spectrograph with 600 lines/mm 750 nm blaze) and a CCD camera (Andor Newton CCD DU920-BX-DD), and the spectra have not been background-corrected or subjected to any further data treatment. We have employed two different methods to achieve plasmonically active Ag and Au tips, known for their spectral response in the visible regime. Ag tips were electrochemically etched in a 1:5 solution of ammonia at 30 % concentration, applying 10 V with a counter electrode of Pt-Ir [14]. For Au tips, a HCl 1:1 solution and 3 V were applied, with a counter electrode of gold. In Fig. 2b we show an example of the electrically-induced plasmon emissionfrom the nanocavity between a Au tip and a Ag(111) surface, cleaned by standard cycles of Ar^+ sputtering and annealing. The intensity of the gap plasmon can be utilized to precisely optimize the collection of light into the optical fiber and spectrometer, and to determine the spectral distribution of the nanocavity plasmonic emission. For that purpose, V_{bias} was set above the voltage threshold, permitting to inelastically excite the plasmon modes of the cavity, and typical currents of ca. 10 nA were sufficient to produce a light intensity observable with a standard CCD camera (Thorlabs CS165CU/M) for integration times around 200 ms. We use a single crystal of a material with a strong plasmonic signal (in our case Ag(111) or Au(111)), in order to observe intense localized surface plasmon resonances (LSPRs) within the visible spectrum (Fig. 2c).

For the tip-enhanced Raman scattering measurements, the crucial condition is the focusing of the laser on the tip-sample junction. A collimated beam reaches the inner lens and can be precisely adjusted using the external X-Y stage, where the collimating lens is installed. The laser spot size is minimized on the body of the tip, close to the junction (Fig. 2d). We use a HeNe laser 632.8 nm (Thorlabs), with a beam diameter of 5 mm after collimation, resulting in a beam spot diameter of <15 μm, as measured on the

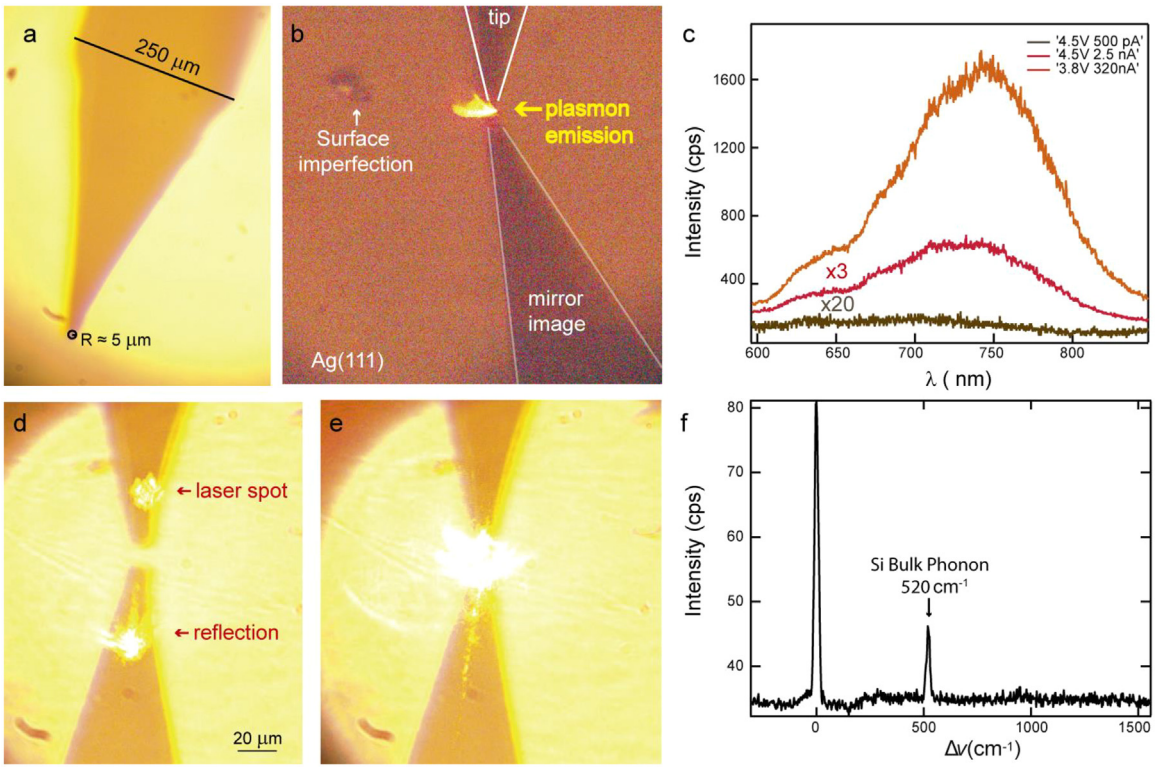

Fig. 2. a) Image of an electrochemically etched Au tip as observed through the lens with a CCD camera. b) Image of the junction at the focus of the lens showing that STML can be observed (STM setpoint: j_{STM}= 100 nA, V_{bias}= 4.0 V, integration time 200 ms). c) STML spectra of a silver tip on a Ag(111) substrate recorded at various setpoints (5 s per spectrum). d) Image of the tip and its mirror image where the laser spot from a 632.8-nm CW source is focused on the tip body and the resulting spot diameter is minimized (< 15 µm). e) Characteristic scattering of the laser focused on the junction. f) Raman spectrum of the silicon surface with the proximity of the tip used to focus the laser (10 s integration time).

body of the tip in the proximity of the tunneling junction. The incident beam is linearly polarized along the tip axis (p-polarization) through the linear polarizer depicted in Fig. 1f. Subsequently, we position the spot on the tip-sample junction (Fig. 2e), with the concomitant fine tuning of the focus to account for the tilted tip axis and geometry. To check the viability of this approach, we first carried out a test experiment with the laser focused on the surface of an unpolished and oxidized silicon wafer mounted on standard flag-style sample support (see Supporting Information Figure S3) and measured the bulk silicon phonon. For the focusing of the laser, we used the body of the tip as described above and then moved the focal point to the surface, observing the bulk phonon mode that is commonly used as a calibration fingerprint for Raman spectroscopy (Fig. 2f).

The TERS benchmark experiment was performed at cryogenic temperatures, for which we prepared a sub-monolayer sample of C_{60} on Ag(111), known to exhibit strong Raman scattering even on non-plasmonic surfaces [15]. C_{60} was purchased from Sigma Aldrich and used without further purification. The molecules were evaporated at 610 K from a Knudsen cell evaporator onto the substrate held at room temperature and subsequently cooled down in the SPM stage to ca. 100 K with a continuous flux of LN_2. The resulting spectrum in the tunneling condition can be observed in Fig. 3a, where the main $A_g(1)$ and $A_g(2)$ vibrational modes of C_{60} are clearly resolved [16,17]. We evaluated the lateral resolution of our system by measuring several Raman spectra along a line on a fullerene cluster (Fig. 3b), being able to resolve the $A_g(2)$ mode with a lateral resolution of ~2 nm (Fig. 3c). Interestingly, the current setup exhibits a promising sensitivity that allows for observation of the anti-Stokes branch of the $A_g(2)$ mode of C_{60} (see Supporting Information Figure S4), crucial to observe local heating phenomena with atomic precision [18,19]. The large enhancement of the anti-Stokes branch, presenting a comparable intensity to the Stokes branch, can be attributed to the spectral distribution of the gap plasmon, as probed by STML, which exhibits higher intensity in the respective region (see Supporting Information Figure S5).

Discussion

We show a simple and economical upgrade of a commercial STM that allows for precise focusing on the tunneling junction with a retractable lens compatible with common bakeout temperatures. Unlike previous modifications that involve costly parabolic mirrors and piezo-motorized components, our approach relies on accessible metal 3D printing with UHV-compatible stainless steel and an affordable plastic lens, resulting in a retractable device that overcomes the key challenge of space limitations near the STM tip-sample junction. Despite the simplicity of the approach, we can perform tip-enhanced spectromicroscopies with ca. 2 nm lateral

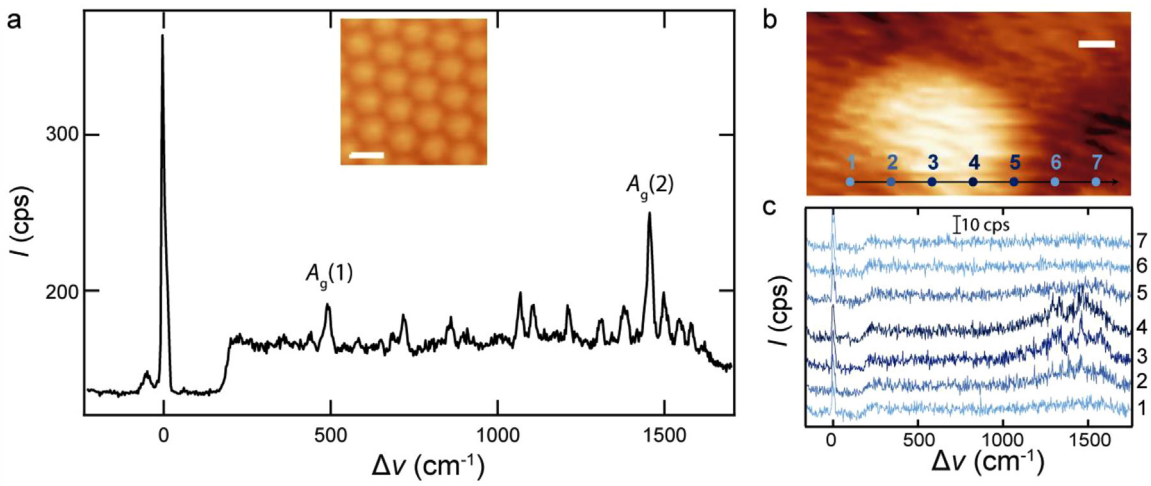

Fig. 3. a) TERS spectrum of a submonolayer sample of C_{60} molecules on Ag(111), showing the characteristic A_g modes among other vibrational frequencies (5 s per spectra, j_{STM}= 100 pA and V_{bias}= −1.0 V). (inset: STM image of a C_{60} monolayer, tunnel conditions 100 pA and −1.0 V, scale bar: 1 nm) b) STM constant-current topography image of a C_{60} cluster on Ag(111). Numbered and colored points represent the location where the spectra in c are recorded with the arrow pointing the measuring direction (scale bar= 2 nm, j_{STM}= 1 nA, V_{bias}= 100 mV). c) Raman spectra acquired every 2 nm over the C_{60} cluster depicted in b (1 s per spectra, j_{STM}= 1.05 nA and V_{bias}= 100 mV). The numbers and colors represent the positions where each spectrum was obtained in panel b.

resolution at cryogenic temperatures. In that sense, it has been shown that the critical aspect of enhancing lateral resolution and sensitivity is the capability to fabricate plasmonic probes with reproducible spectral responses [20]. As previously demonstrated, we suggest that advanced focused ion beam (FIB) nanofabrication has also the potential to largely increase the spectral sensitivity and resolution in our type of system down to the sub-molecular level. The system described in this work permits the operation at lower temperatures using liquid helium, which can further increase the stability of the junction. The increased stability can be exploited to further improve the focus on the junction by tracking the photon-assisted shifting of the field emission resonances [21]. In this regard, low temperatures can also facilitate the exploration of molecular films adsorbed on decoupling layers of ultra-thin film insulators, such as NaCl, allowing to investigate tip-enhanced photoluminescence (TEPL) of single molecules [22,23]. Thus, the versatility of this upgrade holds a great potential for a wide range of optical applications with the widely used Omicron VT-SPM in laboratories worldwide.

Limitations

The current design of a moving lens holder presents some limitations that could be improved to enhance its durability and functionality. One challenge is that the fine tuning of the lens angle, manipulated in vacuum with the wobble stick, leaves the lens exposed to the risk of inflicting scratches during operation on the plastic surface. These scratches can reduce the ability of the lens to inject and collect light at the junction, potentially requiring replacements. This issue could be resolved by replacing the manual nut adjustment with a piezoelectric actuator, enabling a precise remote angle control.

Our design also allows for easy lens replacement to suit specific applications. The plastic aspheric lens is a cost-effective choice and easy to modify, but its limited operational wavelength range reduces the efficiency outside the visible spectrum, hindering its application in UV or near-infrared regions. This issue can be addressed by using alternative optical components optimized for other ranges of the electromagnetic spectrum. These options may need an additional replacement of the borosilicate UHV viewport material to one made of an appropriate material, such as calcium fluoride, zinc selenide, or quartz crystals.

To improve the light detection efficiency, some adjustments are recommended. Currently, our system uses a 90:10 (transmission: reflection) beam splitter to optimize Raman spectroscopy by maximizing light transmission from the junction. For correlation experiments, a 50:50 beam splitter and APD detectors could be installed at perpendicular positions in the cage system, which would reduce the overall costs if the current spectrograph could be replaced with an APD detector.

List of components

Excitation and detection:

Andor Kymera 328i Spectrograph with 600 l/mm 750 blaze
Andor Newton CCD DU920-BX-DD camera with 26 μm pixel size
Thorlabs HNL100RB - HeNe Laser, 632.8 nm, 10 mW, Random polarization
Thorlabs Fiberport collimator PAF2–5A

Optics in UHV:
3D printed Slider (Stainless Steel 316)
3D printed Lens holder (Stainless Steel 316)
3D printed platform with rail (Stainless Steel 316)
Zeonex® E48R Plastic aspheric lens f = 12 mm, diameter: 12 mm
Fine tuning screw and nut (metric M3) (Stainless Steel 316)
Cage system:
Kinematic cage cube for beam splitter DFM1T5
Kinematic blank KM100B/M
2x static cage cubes DFM1B/M
Kinematic Cage Cube Top for right-angle mirror DFM1T4
DFM1/M SM1 Filter Cube
2x fiber adapters SM1FC
X-Y translator CXY1A
X-Y cage CP1XY
Z translator stage SM1ZA
Collimating lens f = 12 mm, diameter= 12 mm
Focusing lens AC254–030-AB-ML
Camera S165CU/M CMOS
8x Rods ER4-P4
Multimode fiber: Thorlabs M43L02
Single mode fiber: P1–630A-FC-2
Linear polarizer LPVISC100-MP2
Plate Beamsplitter BSX10R 25 × 36 mm 10:90 (R:T)
Notch filter: NF633–25
Right angle mirror: MRA25-G01
Cage cube connector C4W-CC
Cage rotation mount CRM1LT/M

Ethics statements

Not applicable.

CRediT author statement

Borja Cirera: Supervision, Conceptualization, Methodology, Validation Analysis and Writing. **Adrián Sáez-Coronado**: Validity test, Sample preparation. **Daniel Arribas**: Sample preparation and Writing. **Javier Méndez**: Resources **Amandeep Sagwal:** Validity tests, Investigation, Tip preparation and Writing, **Rodrigo de Campos Ferreira**: Methodology, Investigation and Writing, **Martin Švec**: Supervision, Funding acquisition, Methodology, Conceptualization and Writing. **Pablo Merino:** Supervision, Funding acquisition, Methodology, Conceptualization and Writing.

Declaration of competing interest

The authors declare that they have no known competing financial interests or personal relationships that could have appeared to influence the work reported in this paper.

Data availability

STEPS files upon request.

Acknowledgments

B. C. acknowledges support from Spanish CM “Talento Program César Nombela” (project No. 2023-T1/TEC-28968). B.C., A. S.-C., D. A., J. M. and P. M. acknowledge support from PID2021–125309OA-100, TED2021–129416A-I00, and CNS2022–135658 funded by MCIN/AEI/10.13039/501100011033 and CSIC-20226AT011. D. A. also acknowledges funding from Spanish MICIN through an FPU-2019 predoctoral grant (FPU19/04556). R.C.C.F, A.S. and M.Š. acknowledge the Czech Science Foundation grant no. 22–18718S and the support from the CzechNanoLab Research Infrastructure supported by MEYS CR (LM2023051). All authors are grateful to Mobility Plus bilateral grant no. BILAT23033/CSIC-24–10 from the Spanish CSIC and the Czech Academy of Sciences.

Supplementary materials

The Supporting Information includes the optical path with and without the inner lens and the integration of the outer optics, the optical schemes of the setups for electro- and TERS/photoluminescence, a picture of the STM junction through the lens on a silicon surface, STM images of submonolayer coverage of C_{60} on Ag(111) and the anti-Stokes and Stokes branches of the spectra with the gap-plasmon spectral distribution

Supplementary material associated with this article can be found, in the online version, at doi:10.1016/j.mex.2025.103156.

References

[1] J. Lee, K.T. Crampton, N. Tallarida, V.A. Apkarian, Nature 568 (2019) 78–82.
[2] J. Xu, X. Zhu, S. Tan, Y. Zhang, B. Li, Y. Tian, H. Shan, X. Cui, A. Zhao, Z. Dong, J. Yang, Y. Luo, B. Wang, J.G. Hou, Science 371 (2021) 818–822.
[3] R. Gutzler, M. Garg, C.R. Ast, K. Kuhnke, K. Kern, Nat. Rev. Phys. 3 (2021) 441–453.
[4] K. Kuhnke, C. Große, P. Merino, K. Kern, Chem. Rev. 117 (2017) 5174–5222.
[5] A. Cahlík, C.C. Müller, F.D. Natterer, MethodsX 13 (2024) 102828.
[6] . https://scientaomicron.com/en/products-solutions/SPM/VT-SPM-Lab.
[7] Y. Xing, S. Bae, E. Ritz, F. Yang, T. Birol, A.N. Capa Salinas, B.R. Ortiz, S.D. Wilson, Z. Wang, R.M. Fernandes, V. Madhavan, Nature 631 (2024) 60–66.
[8] S. Liu, B. Cirera, Y. Sun, I. Hamada, M. Müller, A. Hammud, M. Wolf, T. Kumagai, Nano Lett. 20 (2020) 5879–5884.
[9] H. An, J. Li, Y. Liu, P. Xu, S. Han, Y. Liu, S. Chen, S.-Y. Li, C. Lin, A. Pan, J. Phys. Chem. C 128 (2024) 7583–7590.
[10] S. Liu, M. Müller, Y. Sun, I. Hamada, A. Hammud, M. Wolf, T. Kumagai, Nano Lett. 19 (2019) 5725–7731.
[11] M. Garg, A. Martín-Jiménez, M. Pisarra, Y. Luo, F. Martín, K. Kern, Nat. Photonics 16 (2022) 196–202.
[12] R.L.M Gieseking, J. Lee, N. Tallarida, V. Ara Apkarian, G.C. Schatz, J. Phys. Chem. Lett 9 (2018) 3074–3080.
[13] R.C. de Campos Ferreira, A. Sagwal, J. Doležal, S. Canola, P. Merino, T. Neuman, M. Švec, ACS. Nano 18 (2024) 13164–13170.
[14] C. Zhang, B. Gao, L.G. Chen, Q.S. Meng, H. Yang, R. Zhang, X. Tao, H.Y. Gao, Y. Liao, Z.C. Dong, Review of Scientific Instruments 82 (2011) 083101.
[15] B. Cirera, S. Liu, Y. Park, I. Hamada, M. Wolf, A. Shiotari, T. Kumagai, Phys. Chem. Chem. Phys. 26 (2024) 21325–21331.
[16] J. Menéndez, J. B. Page, in: Light Scattering in Solids VIII, Springer Nature, 2006, pp. 27–95.
[17] B. Cirera, Y. Litman, C. Lin, A. Akkoush, A. Hammud, M. Wolf, M. Rossi, T. Kumagai, Nano Lett. 22 (2022) 2170–2176.
[18] B. Cirera, M. Wolf, T. Kumagai, ACS. Nano 16 (2022) 16443–16451.
[19] Q. Meng, J. Zhang, Y. Zhang, W. Chu, W. Mao, Y. Zhang, J. Yang, Y. Luo, Z. Dong, J.G. Hou, Sci. Adv. 10 (2024) eadl1015.
[20] H. Böckmann, S. Liu, M. Müller, A. Hammud, M. Wolf, T. Kumagai, Nano Lett. 19 (2019) 3597–3602.
[21] S. Liu, M. Wolf, T. Kumagai, Phys. Rev. Lett. 121 (2018) 226802.
[22] K. Kaiser, S. Jiang, M. Romeo, F. Scheurer, G. Schull, A. Rosławska, Phys. Rev. Lett. 133 (2024) 156902.
[23] J. Doležal, A. Sagwal, R.C. de Campos Ferreira, M. Švec, Nano Lett. 24 (2024) 1629–1634.